ChemComm

Negative and zero thermal expansion in α-(Cu2-xZnx)V2O7 solid solutions

Journal:	*ChemComm*
Manuscript ID	CC-COM-06-2020-004505.R1
Article Type:	Communication

COMMUNICATION

Negative and zero thermal expansion in α-$(Cu_{2-x}Zn_x)V_2O_7$ solid solutions

Received 00th January 20xx,
Accepted 00th January 20xx

DOI: 10.1039/x0xx00000x

Naike Shi,[a] Andrea Sanson,[b] Alessandro Venier,[b] Longlong Fan,[c,d] Chengjun Sun, [d] Xianran Xing[a] and Jun Chen*[,a]

Negative or zero thermal expansion (NTE, ZTE) of materials is intriguing for the controllable thermal expansion. We report a series of orthorhombic α-$Cu_{2-x}Zn_xV_2O_7$ (x = 0, 0.1, 0.2), in which the volumetric coefficients of thermal expansion are successful tuned from -10.19×10^{-6} K^{-1} to -1.58×10^{-6} K^{-1} in the temperature range of 100 - 475 K by increasing content of Zn^{2+}. It has been revealed that the transverse vibrations of oxygen bonded with vanadium are dominant the contraction in the *bc* plane leading to the overall volume NTE in α-$Cu_2V_2O_7$. The introduction of Zn^{2+} densifies the crystal structure, which is presumed to suppress the space of transverse vibrations and results in the ZTE in α-$Cu_{1.8}Zn_{0.2}V_2O_7$. This work presents an effective method to realize ZTE in anisotropic framework systems.

Thermal expansion is a conventional phenomenon in solid materials, which is induced by anharmonicity of atom vibrations. The behavior of thermal expansion could be a drawback influencing performance and lifetime when the devices are applied in a large temperature fluctuation environment[1,2]. The discovery of negative thermal expansion (NTE) provides a solution to this problem. A series of NTE materials have been found in the last two decades, including oxides[3-6] fluorides[7,8], nitrides[9,10], alloys[11,12] , Prussian blue analogous[13,14], and metal organic frameworks[15,16]. Diverse factors can induce abnormal NTE, mainly summarized as low frequency transverse motions, charge transfer, magneto volume effect, ferroelectric polarization, and size effect. Usually, transverse motions of atoms dominate the NTE behavior of framework structure materials, in which structure possesses high flexibility benefiting from the existence of corner-shared polyhedra. This kind of material has a relatively wide NTE temperature range compared with electron-driven NTE materials. To satisfy different thermal expansion demands, people try to tune the inherent coefficient of thermal expansion (CTE) in the framework structure NTE materials by the methods of chemical substitution[8,17], local structure distortion[18], and guest molecular or ions intercalation[19,20]. As for the control of thermal expansion, zero thermal expansion (ZTE) is expected to be achieved by proper control of NTE materials to eliminate the influence of thermal expansion.

Most recently, a burgeoning NTE material of $Cu_2V_2O_7$ arouses attention. $Cu_2V_2O_7$ with framework structure has been found to crystallize in four different polymorphs, in which stable α-phase (space group *Fdd2*) and β-phase (space group *C2/c*) were reported to exhibit NTE[5,21-22]. Orthorhombic α-phase shows a volume contraction below 500 K while monoclinic β-phase persists NTE in the whole temperature range. Several works have been carried out to investigate the NTE mechanism and tune the thermal expansion of β-$Cu_2V_2O_7$ by divalent cation substitution for Cu^{2+}, but the volumetric CTE still maintains an obvious negative value which is far from zero[22-24]. Compared with β-$Cu_2V_2O_7$, elaborate studies on the inherent NTE mechanism of α-$Cu_2V_2O_7$ are rare, and it prefers to adopt a monoclinic phase after the chemical substitution[25]. No study on α-$Cu_2V_2O_7$ thermal expansion control has been reported to date as the best of our knowledge.

Herein, a series of α-$Cu_{2-x}Zn_xV_2O_7$ (x = 0, 0.1, 0.2) have been synthesized by an appropriate solid state method. The partial substitution of Cu by Zn can successfully maintain the orthorhombic α-$Cu_2V_2O_7$ phase. The volumetric thermal expansion is tuned from negative to zero with an increasing ratio of Zn substitution from 100K to 475K, and the anisotropy of thermal expansion is reduced. The NTE mechanism of α-$Cu_{2-x}Zn_xV_2O_7$ has been revealed by the combined temperature dependence of high-resolution synchrotron X-ray diffraction (SXRD) and extended X-ray absorption fine structure (EXAFS). It is found that in α-$Cu_2V_2O_7$ the transverse vibration of O atoms,

[a] *Beijing Advanced Innovation Center for Materials Genome Engineering, and Department of Physical Chemistry, University of Science and Technology Beijing, Beijing 100083, China*
[b] *Department of Physics and Astronomy, University of Padova, Padova I-35131, Italy Address here*
[c] *College of Physics and Materials Science, Tianjin Normal University, Tianjin 300387, China*
[d] *Argonne National Laboratory, X-ray Science Division, Argonne, Illinois 60439, United States*
Electronic Supplementary Information (ESI) available: See DOI: 10.1039/x0xx00000x

especially the O atoms bonded with V, gives rise to the coupled rotations of corner-shared VO_4 tetrahedra pairs and edge-shared CuO_5 polyhedra, accounting to the overall NTE. With increasing content of Zn cation with larger size, the free space for O atom transverse vibration and rotation motions of polyhedra in the framework structure is reduced, leading to the weakened NTE along the *b* axis and achieving ZTE in α-$Cu_{1.8}Zn_{0.2}V_2O_7$.

The solid solutions of α-$Cu_{2-x}Zn_xV_2O_7$ (x = 0, 0.1, 0.2) were prepared by the solid state method under the careful controlled condition (see Supporting Information). The crystal structure of α-$Cu_{2-x}Zn_xV_2O_7$ at ambient condition was determined by powder X-ray diffraction (PXRD) and SXRD (Fig. S1). It can be seen that the Zn substituted solid solutions have similar XRD spectra with pure α-$Cu_2V_2O_7$, indicating no phase transition or impurity generated after the Zn substitution. The SXRD patterns of all samples can be refined well with *Fdd2* space group. Fig. S2 illustrates the crystal structure of α-$Cu_{2-x}Zn_xV_2O_7$. The network of α-$Cu_{2-x}Zn_xV_2O_7$ is composed of pairwise corner-connected VO_4 tetrahedra and (Cu/Zn)O_5 zigzag columns formed by edge-shared (Cu/Zn)O_5 distorted quadrangular pyramids. The (Cu/Zn)O_5 columns are aligned to the diagonals of *bc* plane, forming the Cu(Zn)O_5 layers perpendicular to the *a* axis. The layers of (Cu/Zn)O_5 columns are alternately arranged with the (Cu/Zn)O_5 layer A and B along the *a* axis (Fig. S2b). In the same layer the (Cu/Zn)O_5 columns are connected by the VO_4 tetrahedra, while the (Cu/Zn)O_5 layers are linked at both ends of the VO_4 pairs. The lattice parameters of pure α-$Cu_2V_2O_7$ at room temperature are obtained as follows: a = 20.670 Å, b = 8.402 Å, c = 6.444 Å, and V = 1119.141 Å^3. With increasing content of Zn substitution, the unit cell expands along the *a* and *c* axes while shrinks dramatically in the *b* axis, resulting in the overall volume contraction (Fig. S3).

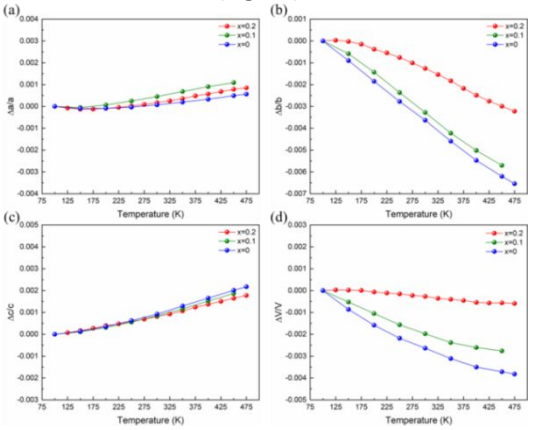

Figure 1. Temperature dependence of lattice parameters of α-$Cu_{2-x}Zn_xV_2O_7$ (x = 0, 0.1, 0.2).

Thermal expansion properties and structure evolutions of α-$Cu_{2-x}Zn_xV_2O_7$ (x = 0, 0.1, 0.2) series were determined by the temperature dependence of SXRD (100 - 475 K). There is no phase transition or decomposition within the measurement temperature range. As shown in Fig. 1, it can be seen that from 100K to 475K α-$Cu_2V_2O_7$ shows positive thermal expansion (PTE) along the *a* and *c* axes, while strong contraction along the *b* axis, resulting in the NTE (α_v ~ -10.19×10^{-6} K^{-1}, 100 - 475K). This anisotropic thermal expansion behavior is in accordance with the previous report[21]. It is intriguing to observe that the introduction of Zn has a very limited impact on the thermal expansion properties of *a* and *c* axes while a strong role in the *b* axis, meaning the suppressive anisotropy thermal expansion. When the amount of Zn reaches 10%, the contraction of *b* axis can counteract the thermal expansion of *a* and *c* axes. Consequently, the volumetric thermal expansion of α-$Cu_{1.8}Zn_{0.2}V_2O_7$ achieves the interesting ZTE over a wide temperature range (α_v ~ -1.58×10^{-6} K^{-1}, 100 - 475K). It is comparable with the ZTE composite of α-$Cu_2V_2O_7$/10wt%Al (α_v ~ -1.47 × 10^{-6} K^{-1}, 300 - 780K)[26], $Zr_{0.5}Hf_{0.5}VPO_7$ (α_v ~ -1.77×10^{-6} K^{-1}, 310 - 673K)[27], and $MgZrF_6$ (α_v ~ -2.38 × 10^{-6} K^{-1}, 300 - 675K)[28]. The detailed CTEs of the three samples are listed in Table S1.

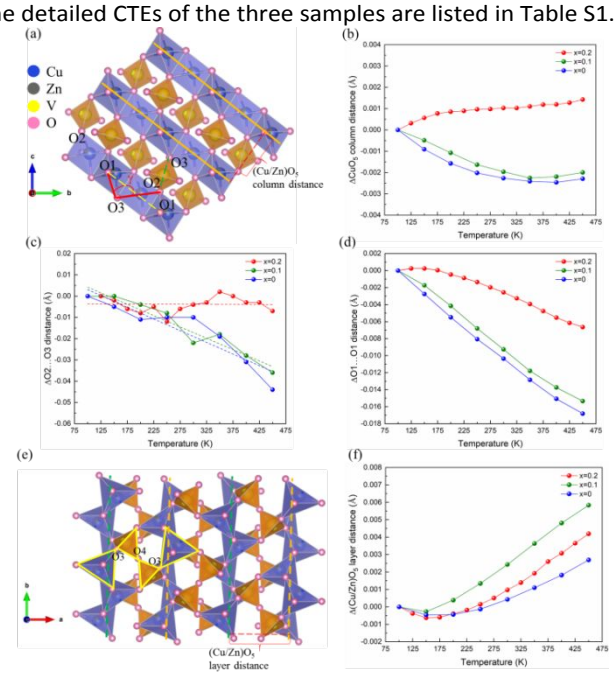

Figure 2. (a) The illustration of crystal structure in a single (Cu/Zn)O_5 layer from the view of the axis *a*. Orange lines refer to the arrangement direction of (Cu/Zn)O_5 columns. The temperature dependence of (b) the adjacent (Cu/Zn)O_5 columns distances, (c) O2⋯O3 distances of VO_4 tetrahedra (the green line in (a)), and (d) O1 ⋯O1 distances of the (Cu/Zn)O_5 columns (the yellow line in (a)). (e) Diagram of (Cu/Zn)O_5 layers from the view of axis *c*. The colored dashed lines refer to the different arrangement directions of (Cu/Zn)O_5 columns. (f) Temperature dependence of adjacent (Cu/Zn)O_5 layers distance.

Why does the unit cell shrink in the direction of the *b* axis and expand along the *a* and *c* axes? According to the feature of crystal structure, it can be analyzed from the aspects of the *bc* plane contraction and the thermal expansion along with *c* axis (Fig. S4a), involving evolutions and rotations among polyhedra. From the view of the axis *a*, (Cu/Zn)O_5 columns are aligned parallel to the diagonal of *bc* face in a (Cu/Zn)O_5 layer (Fig. 2a). It is interesting to find that the distance of adjacent (Cu/Zn)O_5 columns decreases with rising temperature for both x = 0 and 0.1, while for the composition of x = 0.2, the distance variation is small (Fig. 2b). Correspondingly, the edge of O2⋯O3 of VO_4 tetrahedra (the green dotted line in Fig. 2a), which connect the adjacent (Cu/Zn)O_5 columns, shrinks for x = 0 and 0.1, while it maintains a relatively stable value with a slight fluctuation in the

composition of α-$Cu_{1.8}Zn_{0.2}V_2O_7$ (Fig. 2c). Furthermore, the shrinkage of the $(Cu/Zn)O_5$ columns is observed, which is believed to be related to polyhedra rotations. The CuO_5 polyhedra rotation can be indicated by the decreasing degree of angle O1-O3-O2 (the red angle γ in Fig. 2a, Fig. S4b). The rotation motions can lead to the compression of zigzag $(Cu/Zn)O_5$ columns, as reflected by the reduction of O1···O1 (Fig. 2d). Consequently, the $(Cu/Zn)O_5$ columns evolution results in the contracted trend of the area of the *bc* plane, and by comparison, the introduction of Zn^{2+} reduces the related structure evolutions

On the contrary, the separation of neighboring $(Cu/Zn)O_5$ layers along the *a* axis becomes expanded when heating up (Fig. 2e and f). As the linkage between $(Cu/Zn)O_5$ layers, corner-connected VO_4 pairs are straightened, as evidenced by increasing degree of angle O3-O4-O3 (Fig. S5). Straightened VO_4 pairs push the neighboring $(Cu/Zn)O_5$ layers away, which correlates very well with the expansion of unit cell parameter *a* (Fig. 1a).

The behavior of polyhedral units is studied for further investigation. Different from "rigid unit modes" (RUM) which is often applied to explain NTE in framework structure[29], in α-$Cu_{2-x}Zn_xV_2O_7$, $(Cu/Zn)O_5$ and VO_4 polyhedra are not rigid during heating. As shown in Fig. S6 (a) and (b), the volume of $(Cu/Zn)O_5$ expands obviously, while that of VO_4 tetrahedra shrinks with increasing temperature. With increasing content of Zn, the volume of $(Cu/Zn)O_5$ performs the fastest increase rate, with VO_4 volume decreasing with a relatively slower rate for x = 0.2. These results suggest that with increasing content of Zn the volume of polyhedra is more likely to expand, which may also contribute to the weakened NTE. It needs to be noted that both $(Cu/Zn)O_5$ and VO_4 units are not rigid but show deformations. As shown in Fig. S6c,e, one can see that for the CuO_5 polyhedra of α-$Cu_2V_2O_7$, the length of the side of O3(long)···O3(short) shortens while that of O2(long)···O3(short) elongates, indicating a non-rigid character of CuO_5 polyhedra, which contributes the contraction of the *b*-axis and expansion of the *c*-axis. Similar deformation behavior can also be observed in the VO_4 tetrahedra (Fig. S6d). The above analyses indicate that the volume variations of non-rigid polyhedra are concomitant with internal deformation. Since the expansion in the $(Cu/Zn)O_5$ volume overcomes the shrinkage of the VO_4 volume, the single factor of polyhedral volume evolution fails to the NTE explanation. The rotations between polyhedral mentioned before play a key role leading to the ultimate NTE.

To shed light on the inherent driving force giving rise to the coupled polyhedral rotation of NTE, temperature dependent EXAFS measurements for Cu K-edge and V K-edge of $Cu_2V_2O_7$ were employed. The mean bond length of the four nearest-neighbor O atoms around Cu, and the mean V-O bond length in VO_4 polyhedra have been extracted from EXAFS as well as SXRD (Fig. 3a, b). The thermal expansion of the Cu-O bond is in a similar trend derived from both EXAFS and SXRD. However, it is interesting to find an opposite thermal expansion trend for the V-O bond, where the "apparent" bond length resulting from SXRD shrinks while the "true" bond length determined from EXAFS expands. Such phenomenon is not unusual in those framework structure, such as fluorides and Prussian blue analogues[14,30-31]. It indicates that there is a large transverse vibration of O atoms in VO_4. Then we calculated the atomic mean-square relative displacements (MSRDs) for both Cu-O and V-O bonds to investigate the dynamic vibrations. As shown in Fig. 3c and 3d, one can clearly see that perpendicular MSRD is larger than parallel MSRD in not only Cu-O but also V-O bonds, suggesting the O atoms bonding with Cu or V possess larger transverse vibrations than longitudinal vibrations. It is interesting to find that the transverse vibration in V-O bonds is much more pronounced than that in Cu-O bonds, which can be quantitatively revealed by the anisotropy (γ, perpendicular MSRD / parallel MSRD) of the relative average thermal vibrations of Cu-O and V-O pairs. At 300K the value of γ is around 4.9 for Cu-O while that of V-O is 13.5, which is as large as three times of Cu-O. Consequently, we can obtain that the transverse vibration of O atoms linking V atoms dominates the NTE behavior of α-CuV_2O_7 solid solutions.

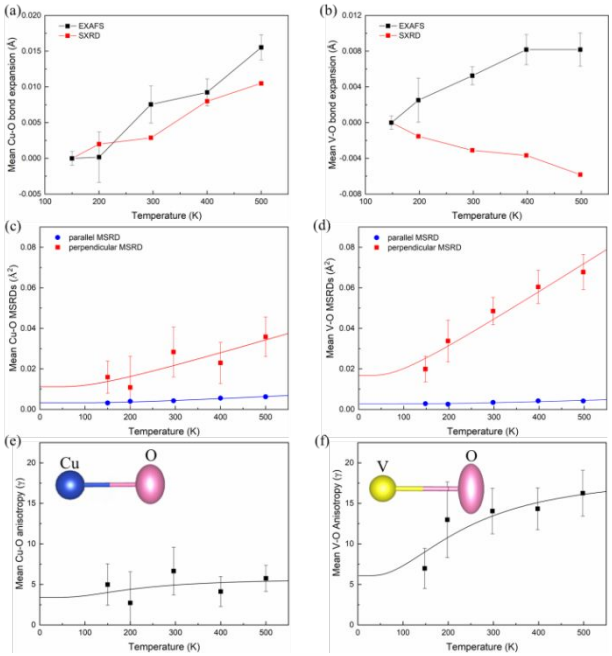

Figure 3. (a) Mean Cu-O bond expansion measured by EXAFS (black symbols) and SXRD (red symbols) (b) Mean V-O bond expansion measured by EXAFS (black symbols) and SXRD (red line). Parallel and perpendicular MRSDs of (c) Cu-O and (d) V-O pairs of $Cu_2V_2O_7$. Anisotropy of the relative average thermal vibrations of (e) Cu-O and (f) V-O pairs in $Cu_2V_2O_7$. The solid lines are the corresponding best-fitting with an Einstein model. The insets are schematics of average thermal vibrations of Cu-O and V-O bonds, respectively.

Empirically, in many framework NTE systems, the chemical substitution by larger ions leads to an increase in the unit cell volume, and NTE can be enhanced in a given structure[8,32-34,]. However, in the present α-$Cu_{2-x}Zn_xV_2O_7$ system the unit cell volume decreases linearly by the chemical substitution of lager Zn^{2+} (r_{Zn2+}=0.82Å) for smaller Cu^{2+} (r_{Cu2+} = 0.79 Å) (Fig. S3). It is deduced that the structure becomes denser after the Zn substitution. Most recently, a new concept of average atomic volume (AAV) was proposed that in those framework materials the NTE is suppressed as the value of AAV decreases[31]. Obviously, in the present α-$Cu_{2-x}Zn_xV_2O_7$ system the value of AAV is reduced by the chemical substitution of Zn. In addition,

the volume of CuO_5 and VO_4 polyhedra expand after the introduction of Zn (Fig. S6), which also means the free space outside the polyhedra is reduced. As a result, the free space for atom dynamic vibrations is compressed, which inhibits the flexibility of structure and results in weakened NTE.

In conclusion, thermal expansion from negative to zero has been realized in the α-$Cu_{2-x}Zn_xV_2O_7$ solid solutions from 100 to 475K. It is the first time to reveal the NTE mechanism of α-$Cu_2V_2O_7$ from the perspective of atomic dynamic vibration by joint SXRD and EXAFS analyses. It is found that transverse vibrations of O atoms exist in the Cu-O and V-O bonds, in which those O atoms bonded with V show dominating role of transverse vibrations to NTE. The coupled rotations occur among the non-rigid polyhedra, which brings the shrinkage of the *bc* plane and accounts to the anisotropic NTE. Chemical substitution of small Cu by large Zn reduces the value of AAV, which decreases the free space for the transverse vibrations. Ultimately, the NTE of the *b* axis of α-$Cu_{1.8}Zn_{0.2}V_2O_7$ is much weakened to achieve the interesting ZTE.

This work was supported by the National Natural Science Foundation of China (grant nos. 21825102, 21731001, and 21590793), and the Fundamental Research Funds for the Central Universities, China (FRF-TP-18-001C2). Use of the Advanced Photon Source, an Office of Science User Facility operated for the U.S. Department of Energy (DOE), Office of Science, by Argonne National Laboratory, was supported by the U.S. DOE under contract no. DE-AC02-06CH11357. We acknowledge Advanced Photon Source for provision of synchrotron radiation as well as all the staff of Beamline 11-BM-B, 20-BM-B and 12-BM-B for technical assistance. J.C. acknowledges the financial support of the University of Padova through the Visiting Scientist program 2019.

Conflicts of interest

There are no conflicts to declare.

Notes and references

1 J. S. Evans, Dalton. Trans., 1999, 3317-3326.
2 K. Takenaka, Sci. Technol. Adv. Mat., 2012, 13, 013001.
3 T. Mary, J. Evans, T. Vogt and A. Sleight, Science, 1996, 272, 90-92.
4 J. Evans, T. Mary and A. Sleight, J. Solid State Chem., 1998, 137, 148-160.
5 H. Wang, M. Yang, M. Chao, J. Guo, Q. Gao, Y. Jiao, X. Tang and E. Liang, Solid. State. Ion., 2019, 343, 115086.
6 N. Shi, A. Sanson, Q. Gao, Q. Sun, Y. Ren, Q. Huang, D. O. de Souza, X. Xing and J. Chen, J. Am. Chem. Soc., 2020, 142, 3088-3093.
7 B. K. Greve, K. L. Martin, P. L. Lee, P. J. Chupas, K. W. Chapman and A. P. Wilkinson, J. Am. Chem. Soc., 2010, 132, 15496-15498.
8 L. Hu, J. Chen, J. Xu, N. Wang, F. Han, Y. Ren, Z. Pan, Y. Rong, R. Huang and J. Deng, J. Am. Chem. Soc., 2016, 138, 14530-14533.
9 Y. Sun, C. Wang, Y. Wen, L. Chu, H. Pan, M. Nie and M. Tang, J. Am. Ceram. Soc., 2010, 93, 2178-2181.
10 H. Lu, Y. Sun, S. Deng, K. Shi, L. Wang, W. Zhao, H. Han, S. Deng and C. Wang, J. Am. Ceram. Soc., 2017, 100, 5739-5745.
11 M. van Schilfgaarde, I. Abrikosov and B. Johansson, Nature, 1999, 400, 46-49.
12 J. H. Belo, A. L. Pires, I. T. Gomes, V. Andrade, J. B. Sousa, R. L. Hadimani, D. C. Jiles, Y. Ren, X. Zhang and J. P. Araújo, Phys. Rev. B, 2019, 100, 134303.
13 S. Margadonna, K. Prassides and A. N. Fitch, J. Am. Chem. Soc., 2004, 126, 15390-15391.
14 N. Shi, Q. Gao, A. Sanson, Q. Li, L. Fan, Y. Ren, L. Olivi, J. Chen and X. Xing, Dalton. Trans., 2019, 48, 3658-3663.
15 Y. Wu, A. Kobayashi, G. J. Halder, V. K. Peterson, K. W. Chapman, N. Lock, P. D. Southon and C. J. Kepert, Angew. Chem. Int. Ed., 2008, 47, 8929-8932.
16 M. J. Cliffe, J. A. Hill, C. A. Murray, F.-X. Coudert and A. L. Goodwin, Phys. Chem. Chem. Phys., 2015, 17, 11586-11592.
17 K. Takenaka, T. Shinoda, N. Inoue, Y. Okamoto, N. Katayama, Y. Sakai, T. Nishikubo and M. Azuma, Appl. Phys. Express, 2017, 10, 115501.
18 L. Hu, F. Qin, A. Sanson, L.-F. Huang, Z. Pan, Q. Li, Q. Sun, L. Wang, F. Guo and U. Aydemir, J. Am. Chem. Soc., 2018, 140, 4477-4480.
19 Q. Gao, J. Chen, Q. Sun, D. Chang, Q. Huang, H. Wu, A. Sanson, R. Milazzo, H. Zhu and Q. Li, Angew. Chem. Int. Ed., 2017, 56, 9023-9028.
20 J. E. Auckett, A. A. Barkhordarian, S. H. Ogilvie, S. G. Duyker, H. Chevreau, V. K. Peterson and C. J. Kepert, Nat. Commun., 2018, 9, 1-5.
21 N. Zhang, L. Li, M. Wu, Y. Li, D. Feng, C. Liu, Y. Mao, J. Guo, M. Chao and E. Liang, J. Eur. Ceram. Soc., 2016, 36, 2761-2766.
22 N. Katayama, K. Otsuka, M. Mitamura, Y. Yokoyama, Y. Okamoto and K. Takenaka, Appl. Phys. Lett., 2018, 113, 181902.
23 H. Wang, M. Yang, M. Chao, J. Guo, X. Tang, Y. Jiao and E. Liang, Ceram. Int., 2019, 45, 9814-9819.
24 M. Rotermel, T. Krasnenko, S. Titova and S. Praynichnikov, J. Solid State Chem., 2020, 285, 121221.
25 T. Krasnenko, S. Petrova, R. Zakharov, O. Sivtsova and A. Chvanova, Russ. J. Inorg. Chem., 2008, 53, 1641-1647.
26 N. Zhang, Y. Mao, X. Liu, M. Yang, X. Kong, M. Zhang, X. Kong, J. Guo, M. Chao and E. Liang, Ceram. Int., 2016, 42, 17004-17008.
27 J.-P. Wang, Q.-D. Chen, S.-L. Li, Y.-J. Ji, W.-Y. Mu, W.-W. Feng, G.-J. Zeng, Y.-W. Liu and E.-J. Liang, Chin. Phys. B., 2018, 27, 066501.
28 J. Xu, L. Hu, Y. Song, F. Han, Y. Qiao, J. Deng, J. Chen and X. Xing, J. Am. Ceram. Soc., 2017, 100, 5385-5388.
29 A. K. Pryde, K. D. Hammonds, M. T. Dove, V. Heine, J. D. Gale and M. C. Warren, Phase. Transit., 1997, 61, 141-153.
30 L. Hu, J. Chen, A. Sanson, H. Wu, C. Guglieri Rodriguez, L. Olivi, Y. Ren, L. Fan, J. Deng and X. Xing, J. Am. Chem. Soc., 2016, 138, 8320-8323.
31 Q. Gao, J. Wang, A. Sanson, Q. Sun, E. Liang, X. Xing and J. Chen, J. Am. Chem. Soc., 2020, 142, 6935-6939.
32 K. W. Chapman, P. J. Chupas and C. J. Kepert, J. Am. Chem. Soc., 2006, 128, 7009-7014
33 G. Wallez, P. E. Raison, N. Dacheux, N. Clavier, D. Bykov, L. Delevoye, K. Popa, D. Bregiroux, A. N. Fitch and R. J. Konings, Inorg. Chem., 2012, 51, 4314-4322.
34 C. Lind, Materials, 2012, 5, 1125-1154.